Damping of Inter-area Oscillations using Energy Storage

Jason C. Neely, *Member, IEEE,* Raymond H. Byrne, *Senior Member, IEEE,* Ryan T. Elliott, *Member, IEEE,* César A. Silva-Monroy, *Member, IEEE,* David A. Schoenwald, *Senior Member, IEEE,* Daniel J. Trudnowski, *Fellow, IEEE* and Matthew K. Donnelly, *Senior Member, IEEE*

***Abstract*—Low frequency inter-area oscillations have been identified as a significant problem in utility systems due to the potential for system damage and the resulting restrictions on power transmission over select lines. Previous research has identified real power injection by energy storage based damping control nodes as a promising approach to mitigate inter-area oscillations. In this paper, a candidate energy storage system based on UltraCapacitor technology is evaluated for damping control applications in the Western Electric Coordinating Council (WECC), and an analytical method for ensuring proper stability margins is also presented for inclusion in a future supervisory control algorithm. Dynamic simulations of the WECC were performed to validate the expected system performance. Finally, the Nyquist stability criteria was employed to derive safe operating regions in the gain, time delay space for a simple two-area system to provide guaranteed margins of stability.**

***Index Terms*—Inter-area oscillations, WECC, energy storage applications, damping control**

I. Introduction

INTER-AREA oscillations may result when large generation and load complexes are separated by long transmission lines. In a large power system, such as the Western Interconnection, these oscillations are typically between 0.2 and 1.0 Hz and may persist for extended periods due to low damping. There is a large economic motivation for mitigating these oscillations. First, low frequency oscillations can lead to a system breakup if the damping becomes too low. Second, the power flow down some transmission lines is limited to preserve small signal stability. Improving the small signal stability allows higher power flows, which has a measurable economic benefit.

Multiple approaches have been proposed for damping inter-area oscillations. In [1], [2], researchers investigated modulation of static VAR compensators (SVC) for damping control using active power flow as the control input. A proposed SVC system for the Nordic power grid is described in [3]; operational testing of the Nordic system is currently under way. Modulation of the PDCI was proposed in [4]. Other potential methods include thyristor braking and series impedance modulation. The destabilizing effect of communications latency is discussed in [4], [5].

J. Neely, R. Byrne, R. Elliott, C. Silva-Monry and D. Schoenwald are with Sandia National Laboratories, Albuquerque, NM, 87123 e-mail: jneely@sandia.gov.

D. Trudnowski and M. Donnelly are with Montana Tech, Electrical Engineering Department, 1300 W. Park Street, Butte, MT 59701

Manuscript received December 7th , 2012

The damping control approach proposed herein builds on the results given in [6]. Two damping control systems are installed in areas expected to oscillate against one another, and real power is injected at each location based on the frequency error between the two nodes. This control is presented in detail in Section II. In Section III, a candidate energy storage system based on UltraCapacitor technology is described and modeled. In Section IV, the damping control is applied in simulation to a Western Electric Coordinating Council (WECC) base case using General Electric's Positive Sequence Load Flow (PSLF) software. Therein, the benefits of damping control and the potential hazards of communication latency are demonstrated in simuatlion. In Section V, an analytical approach based on Nyquist is presented for maintaining stability margins in the damping controllers. Finally, conclusions are given in Section VI.

II. Oscillation Damping using Real Power Modulation

The controller block diagram is shown in Figure 1 [6]; it includes two *damping controllers* located in different areas, a communication link, and a *supervisory controller* that oversees the control. The damping controllers operate by sourcing or syncing power in each area proportional to the frequency difference between areas. Specifically, a frequency measurement in one area must be made and communicated in real time to the other area. Ideally, the communication delays are minimal or at least constant; in practice, however, communication latencies can be significant and variable. Herein, the latency associated with a local frequency measurement is neglected; delays for remote measurements are accounted for but assumed to be equal in each direction. The control law for each damping control node is given as

$$P_1^*(t) = -K_d\left(f_1(t) - f_2(t - T_d)\right) \quad (1)$$

$$P_2^*(t) = -K_d\left(f_2(t) - f_1(t - T_d)\right) \quad (2)$$

where P_1^* and P_2^* are the powers commanded by the damping controller at each node in MW, f_1 and f_2 are the frequencies measured in mHz in areas 1 and 2, K_d is the control gain in MW/mHz and communication delay is given by T_d in seconds.

III. Candidate Energy Storage System

The control given by equations (1) and (2) requires two energy storage based controllers be installed at oscillation

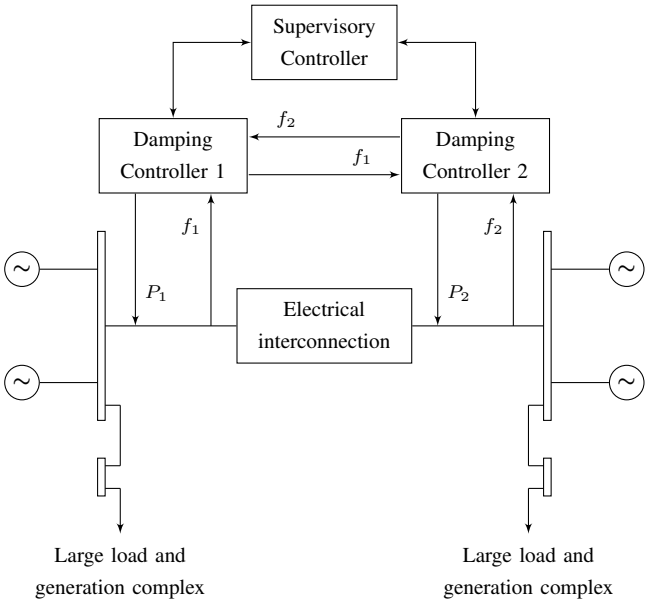

Fig. 1. Two area system with damping control [6]

nodes in the system. In this section, a practical candidate system is described for which a detailed full state model was generated to represent the storage system dynamics including: filter inductor currents, filter capacitor voltages, transformer reactances, ultracapacitor voltage and the control integrator. Finally, the performance of the detailed model is compared to a first order approximation to aid in the development of a representative, but numerically tractable, PSLF model that can be used for simulation in WECC studies.

A. System Description

The energy storage system considered herein utilizes ten Maxwell Technologies 125V Heavy Transportation modules connected in series. The modules use ultracapacitor technology and each have a rated voltage of 125V with a rated capacitance of 63F; the resulting system is rated for 1250V, 6.3F. The ultracapacitor is modeled as an ideal capacitor with equivalent series resistance (ESR) r_c and leakage resistance r_{leak} and connects to the utility through a bidirectional DC/AC converter with step-up Δ-Y transformer; see Figure 2. Filter components L_f, C_f were selected for >15 kHz switching. To perform the damping control, reference powers P_1^*, P_2^* are determined using (1) and (2), and a simple proportional+integral (PI) controller is implemented in each to drive $P_1 \rightarrow P_1^*$, $P_2 \rightarrow P_2^*$.

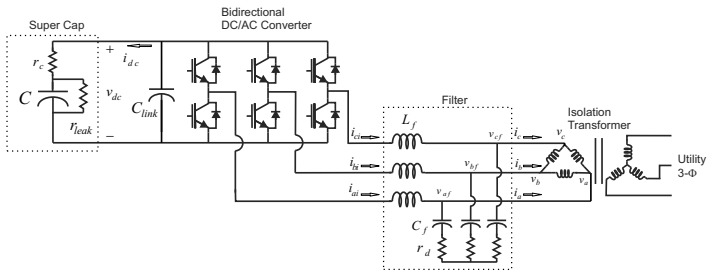

Fig. 2. UltraCapacitor Energy Storage System

B. PI Feedback Control of Inverter

Control of the power intput or output of the inverter is accomplished using a PI control applied to the *qd* variables of the system [7]. For a d-axis grid voltage of $v_d = 0$ and commanded real and reactive powers P^* and Q^*, the power command is used to determine commanded currents

$$i_q^* = \frac{2}{3}\frac{P^*}{v_q}, i_d^* = \frac{2}{3}\frac{Q^*}{v_q} \tag{3}$$

Herein, we assume that $Q^* = 0$, resulting in $i_d^* = 0$. Subsequently, measured currents are transformed into *qd0* variables, and reference inverter voltages are computed according to the PI control [7] :

$$v_{qi}^* = v_q + Xi_d + \left(K_p + \frac{K_i}{s}\right)\left(i_q^* - i_q\right) \tag{4}$$

$$v_{di}^* = v_d - Xi_q + \left(K_p + \frac{K_i}{s}\right)\left(i_d^* - i_d\right) \tag{5}$$

where $X = \omega_e(L_f + L_g)$. The impedance of the filter capacitor is assumed to be sufficiently large at 60 Hz to be neglected. The reference *qd0* voltages are then transformed back into *abc* variables and realized using sine-triangle modulation. If the modulation scheme performs as intended, wherein $v_{qi} \rightarrow v_{qi}^*$ and $v_{di} \rightarrow v_{di}^*$, then output current and current reference are related by

$$\frac{i_x^*(s)}{i_x(s)} = \frac{K_p}{(L_f + L_g)} \frac{\left(s + \frac{K_i}{K_p}\right)}{\left(s^2 + \frac{r_g + r_f + K_p}{L_f + L_g}s + \frac{K_i}{L_f + L_g}\right)} \tag{6}$$

where i_x can represent the q or d axis current. Equation 6 allows for placement of the closed loop poles λ_1 and λ_2:

$$K_p = -(L_f + L_g)(\lambda_1 + \lambda_2) - (r_f + r_g) \tag{7}$$

$$K_i = (L_f + L_g)(\lambda_1 \lambda_2) \tag{8}$$

To maintain stability, care must be taken to ensure the Routh-Hurwitz criterion is satisfied, namely that (1) $K_i > 0$ and (2) $r_g + r_f + K_p > 0$. In particular, requirement (2) may be violated if there is a large uncertainty in $r_g + r_f$. To ensure (2) is satisfied and also to avoid a nonminimum phase closed-loop response, it is best that $K_p > 0$. The inverter parameters used in this study are given in Table I.

TABLE I
ENERGY STORAGE SYSTEM PARAMETERS

Parameter Description	Parameter Name	Value	Units
UltraCap Capacitance	C	6.3	Farads
UltraCap ESR	r_c	0.18	Ω
Leakage Resistance	r_{leak}	12.5	kΩ
Filter Inductance	L_f	550	μH
Filter inductor resistance	r_{Lf}	50	mΩ
Filter Capacitance	C_f	20	μF
Damping Resistance	r_d	10	Ω
Grid inductance	L_g	2.0	mH
Inverter Voltage	V_i	360	V RMS
Controller Eigenvalues	λ_1, λ_2	-60	

C. Simplified Inverter Model

To determine the frequency response of the detailed inverter model with controls, the reference power P^* was implemented using a *chirp* signal; the power output to the grid was then evaluated for gain and phase. For comparison, the same was done for a simple first order system with time constant $\tau = 0.01$ seconds. The results are show in Figure 3. It is noted both that the system has sufficient bandwidth to accomplish the control and that the frequency response of the detailed model has good agreement with that of the first order model.

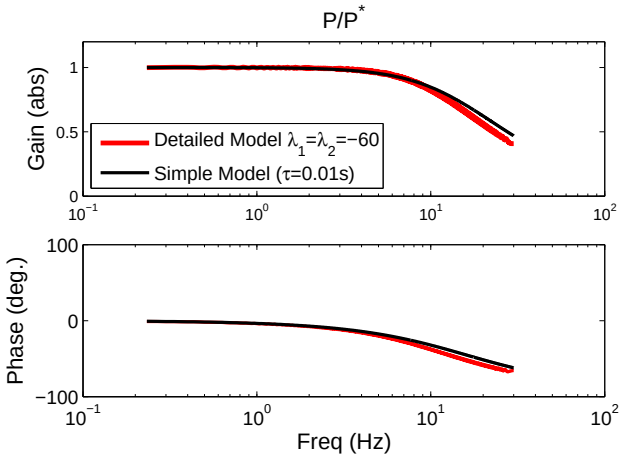

Fig. 3. First Order Approximation of UltraCapacitor Energy Storage System

IV. Simulation Results

Herein, a simulation example is given that applies the candidate UltraCapacitor-based oscillation damping system to mitigate inter-area oscillations on the WECC. First, a custom model of the UltraCapacitor based energy storage system with grid-tied inverter was developed for PSLF; therein, the inverter was modeled using a simple first order approximation and scaled up to represent 10 parallel connected units. In simulation, the system was placed in two locations within an existing PSLF WECC base case having predicted characteristics for 2017 heavy summer. One damping control was connected to a bus in Palo Verde (bus 15021), and the other was connected near Grand Coulee Dam (bus 41356). A transient inter-area oscillation was excited by simulating a fault on a 500kV power line in British Columbia (CBK500) at t=10 seconds.

The response of the system was first considered for variation in K_d. Specifically, as K_d varied from 0 to 4 MW/mHz (with T_d=0), the difference in generator speeds at Palo Verde (PALOVRD2 A14 - bus 14932) and Coulee (COULEE22 A40 - bus 40296) were computed at each gain value and the ring-down response was evaluated using Prony analysis to extract mode frequency and damping information. In each case, the two dominant modes were in the neighborhood of 0.30 Hz and 0.52 Hz. Prony results are shown in Figure 4. Performing a linear fit on the 0.30 Hz mode reveals an approximate 3.1% gain in damping for each MW/mHz increase in K_d. The result for the 0.52 Hz mode is not linear, but a clear benefit is seen in the damping of this mode as well.

In addition, time-domain results are given in Figure 5. For $K_d = 0$, the damping controllers had no effect and the generator speeds in the two areas oscillated against one another for over 20 seconds following the line fault. For K_d = 4 MW/mHz, the oscillations are considerably damped, resulting in an oscillation that lasted approximately 7 seconds. When a modest time delay of T_d= 1 second is introduced however, much of the benefit of the damping control is negated, apparently causing the damping now to decrease.

Effects of the damping controllers are not isolated to these two areas; effects are observed on generators across the WECC. In Figure 6, the generator speeds for five generators running south to north between the two damping nodes are shown. It is apparent that this system can significantly impact small signal response across the WECC.

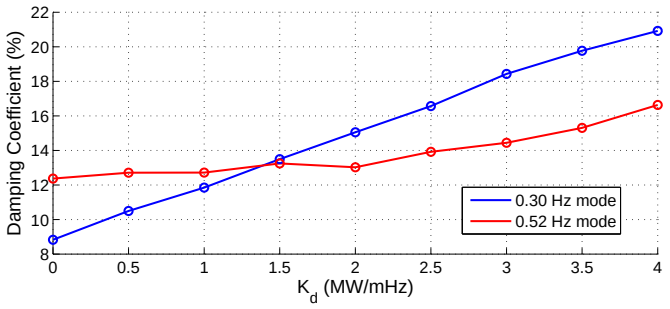

Fig. 4. Damping coefficient (%) versus K_d (MW/mHz) for dominant modes, with T_d=0

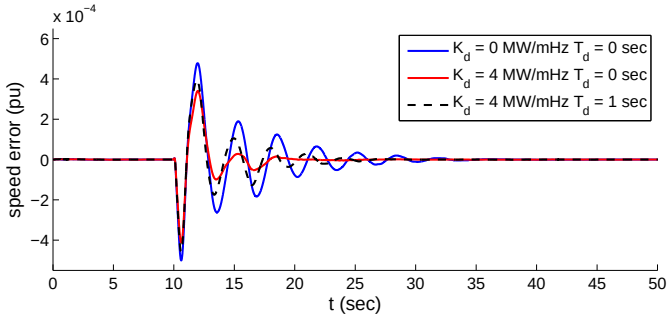

Fig. 5. Generator speed difference: PALOVRD2 A14 - COULEE22 A40

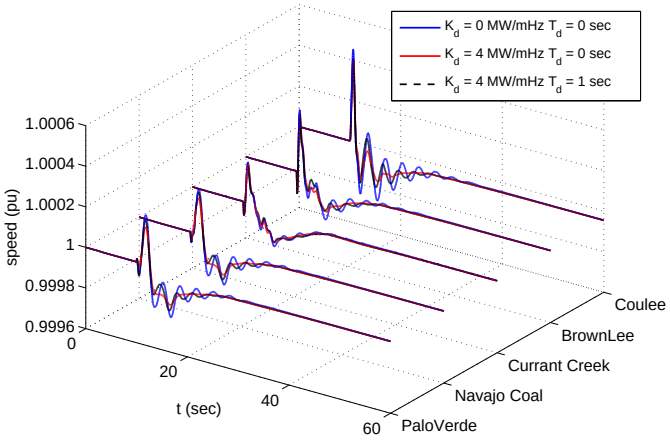

Fig. 6. Generator speeds at 5 buses in the WECC with variation in K_d, T_d

V. Supervisory Control

Energy storage systems must be equipped with a supervisory control that monitors the health of the energy storage components and power electronics interface. This supervisory control typically maintains the system within voltage, current, power, and temperature limits and monitors its operation, disabling it at the first sign of trouble. For the application presented herein, the energy storage system is specifically designed to augment the small signal behavior of the grid. Thus, an additional supervisory layer must be implemented to ensure system stability. In particular, large gains combined with large communication delays can lead to decreased damping and ultimately, in some cases, system instability. In [8], an analytical method termed the *ESAC criterion* (named for the Energy Systems Analysis Consortium) was used to establish modes of operation that ensure margins of stability in power electronic systems. Herein, the ESAC criterion is extended to consider the combined effect of K_d and T_d on margins of stability in a two-area damping control example.

A. ESAC Criterion

The Nyquist criterion is a fundamental tool for establishing stability. By generating a *Nyquist diagram* for the open-loop function $G(s)H(s)$ with P right-half plane (RFP) poles and counting the number of clockwise encirclements of the -1 point (N), one may calculate the number of RHP closed-loop poles, $Z = N + P$ and thus establish if a system is stable [9]. However, an added strength of the Nyquist method is the ability to relate the shape of the Nyquist diagram to margins of stability. There have been several design methods that establish stability margins by bounding the Nyquist contour such as the *Middlebrooke criterion* and the *Gain Margin Phase Margin criterion*; however, these are considered to be overly conservative [8]. The ESAC criterion was designed to reduce conservativeness.

Herein, the ESAC criterion is implemented in five steps. The first step is to identify the system model in the frequency domain. The second is to identify a suitable gain margin (GM) and phase margin (Φ_m) and compute $\alpha^* = 10^{-GM/20}$. Third, using Φ_m and α^* values, identify the ESAC boundary lines in the frequency plane as shown in Figure 7. Specifically, four lines are drawn to define the boundary. Two lines extend from the point $(-\alpha^*, 0)$ to where lines of angle $\pm\Phi_m$ intersect the unit circle. Two additional lines extend from these intersection points horizontally to negative infinity. In the fourth step, the ESAC boundary lines are mapped to *forbidden regions* in $K_d(1 + e^{-T_d s_a})$ for a set of s_a values. Finally, forbidden regions in $K_d(1 + e^{-T_d s_a})$ are combined and mapped to the (T_d, K_d) space.

B. Example Two-area system

To demonstrate application of the ESAC criterion, a simple two-area system is considered. See Figure 8 adapted from [10] to include small-signal damping powers

$$\Delta P_{D1}(s) = -K_d\left(\Delta\omega_1(s) - \Delta\omega_2(s)e^{-T_d s}\right) \quad (9)$$

$$\Delta P_{D2}(s) = -K_d\left(\Delta\omega_2(s) - \Delta\omega_1(s)e^{-T_d s}\right) \quad (10)$$

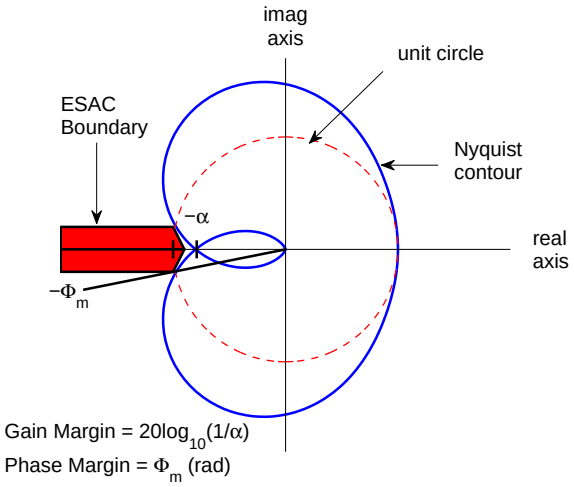

Fig. 7. ESAC Boundary for Specified Gain and Phase Margin

where all quantities including K_d are in per-unit for this example. The rotational dynamics and governor/turbine dynamics are identical for each area and given as [10]:

$$G(s) = \frac{1}{M_1 s + D_1} = \frac{1}{M_2 s + D_2} \quad (11)$$

$$C(s) = \frac{1}{T_g s + 1} \cdot \frac{T_r s + 1}{(R_t/R_p)T_r s + 1} \cdot \frac{1 - sT_w}{1 + 0.5T_w s} \quad (12)$$

For this example, the transfer function relating the difference in frequency to the difference in load in the two areas is

$$\frac{\Delta\overline{\omega}(s)}{\Delta\overline{P_L}(s)} = \frac{G(s)}{1 + G(s)\left(\frac{C(s)}{R_p} + \frac{2T}{s} + K_d(1 + e^{-T_d s})\right)} \quad (13)$$

where $\Delta\overline{\omega}(s) = \Delta\omega_1(s) - \Delta\omega_2(s)$ and $\Delta\overline{P_L}(s) = \Delta P_{L1}(s) - \Delta P_{L2}(s)$ and T is the synchronizing torque defined as follows:

$$T = \frac{\Delta P_{12}}{\Delta\delta_{12}} = \frac{V_1 V_2}{X_T}\cos(\delta_{12}) \quad (14)$$

where P_{12} is the power transmitted from area 1 to area 2, V_1 and V_2 are the voltages at the respective end points of the tie line, $\delta_{12} = \delta_1 - \delta_2$ is the difference in electrical angles, and X_T is the total reactance of the transmission tie connecting both areas [10]. For this example, δ_{12}=0.3047 (corresponding to P_{12}=1.0), X_T = 0.30, and $M_1 = M_2 = 5.0$. For the sake of brevity, the remaining parameter values are not listed, but descriptions of these parameters and their values are found in [10] page 599.

C. Gain Scheduling in Delay-Gain Space

To begin, we select our margins to be GM = 3 dB and $\Phi_m = 9^\circ$ and establish the ESAC boundary. Then, the open loop function from (13) is equated with s_b on the ESAC boundary

$$G(s_a)\left(\frac{C(s_a)}{R_p} + \frac{2T}{s_a} + K_d\left(1 + e^{-T_d s_a}\right)\right) = s_b \quad (15)$$

where $s_a = j\omega_a$ corresponds to system frequency ω_a in radians/second. Rearranging (15) gives the following

$$K_d\left(1 + e^{-T_d s_a}\right) = \frac{s_b}{G(s_a)} - \frac{C(s_a)}{R_p} - \frac{2T}{s_a} \quad (16)$$

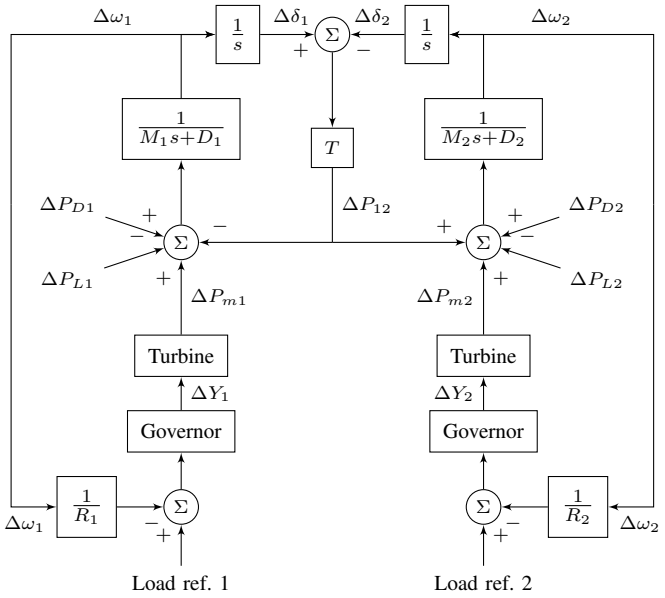

Fig. 8. Two area system control diagram (adapted from [10])

For each s_a, lines of the ESAC boundary are mapped using (16) to outline *forbidden regions* for $K_d(1 + e^{-T_d s_a})$. An example is given in Figure 9 for $s_a = 1.171\pi j$.

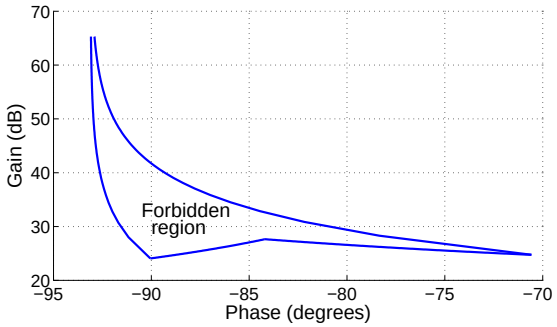

Fig. 9. Forbidden region for $K_d\left(1 + e^{-T_d s_a}\right)$ at $s_a = 1.171\pi j$

The phase (in radians) and magnitude of $K_d(1 + e^{-T_d s_a})$ are used to compute forbidden regions in (T_d, K_d) space using

$$T_d = \frac{-2 \cdot \angle\left[K_d(1 + e^{-T_d s_a})\right]}{\omega_a}, K_d = \frac{|K_d\left(1 + e^{-T_d s_a}\right)|}{|1 + e^{-T_d s_a}|} \quad (17)$$

The forbidden regions for all s_a values are then plotted together in the (T_d, K_d) plane; see Figure 10. It is noted that the top points of each forbidden region go to positive infinity, and a continuum between regions is inferred. Therefore, in this example, the "nose-shaped" region near the origin constitutes our set of allowable (T_d, K_d) values.

VI. Conclusions

In this paper, the damping control method proposed in [6] is realized in simulation using energy storage. Specifically, a candidate energy storage system based on UltraCapacitors is designed and modeled in PSLF. Simulations of the damping controller applied to a WECC base case indicate significant and predictable improvement in the damping of inter-area oscillations. However, results also indicate that communication latency may reduce damping. To mitigate this issue, the ESAC stability criterion [8] was extended to consider communication delay, and preliminary results were attained for a two-area system example. Development of a supervisory control scheme based on this analysis is the subject of ongoing work. Nonetheless, the results presented herein reinforce the feasibility and potential value of energy storage based damping control.

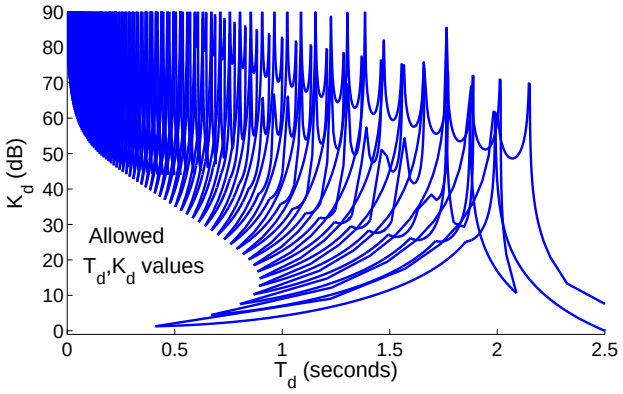

Fig. 10. Forbidden areas for each frequency shown in (T_d, K_d) space

Acknowledgment

The research was performed with funding provided by the DOE Energy Storage Program managed by Dr. Imre Gyuk of the DOE Office of Electricity Delivery and Energy Reliability. We thank Dr. Gyuk for his support and guidance on this effort.

Sandia National Laboratories is a multi-program laboratory managed and operated by Sandia Corporation, a wholly owned subsidiary of Lockheed Martin Corporation, for the U.S. Department of Energy's National Nuclear Security Administration, under contract DE-AC04-94AL85000.

References

[1] J. Q. Restrepo, *A Real-Time Wide-Area Control for Mitigating Small-Signal Instability in Large Electric Power Systems*. PhD thesis, Washington State University, May 2005.

[2] J. Quintero and V. M. Venkatasubramanian, "A real-time wide-area control framework for mitigating small-signal instability in large electric power systems," in *Proceedings of the* 38^{th} *Hawaii International Conference on System Sciences*, pp. 66–75, January 2005.

[3] N. Chaudhuri, A. Domahidi, R. Majumder, B. Chaudhuri, P. Korba, S. Ray, and K. Uhlen, "Wide-area power oscillation damping control in nordic equivalent system," *Generation, Transmission Distribution, IET*, vol. 4, pp. 1139 –1150, October 2010.

[4] D. J. Trudnowksi, "Appendix 3: Analytical assessment of proposed controls," tech. rep., Report to Bonneville Power Administration, Portland, OR, 2008.

[5] J. He, C. Lu, X. Jin, and P. Li, "Analysis of time delay effects on wide area damping control," in *Proceedings of the 2008 IEEE Asia Pacific Conference on Circuits and Systems*, pp. 758–761, December 2008.

[6] J. Undrill, "Investigation of asymptotic stability of low frequency oscillations," tech. rep., Report to Bonneville Power Administration, Portland, OR, 2010.

[7] P. C. Krause, O. Wasynczuk, and S. Sudhoff, *Analysis of Electric Machinery and Drive Systems*. Piscataway, NJ: IEEE Press, John Wiley and Sons, Inc., second ed., 2002.

[8] S. Sudhoff, S. Glover, P. Lamm, D. Schmucker, and D. Delisle, "Admittance space stability analysis of power electronic systems," *Aerospace and Electronic Systems, IEEE Transactions on*, vol. 36, pp. 965–973, July 2000.

[9] C. L. Phillips and R. D. Harbor, *Feedback Control Systems*. Saddle River, NJ: Prentice Hall, 1996.

[10] P. Kundur, *Power System Stability and Control*. New York: McGraw-Hill, Inc., 1993.